Available online at www.sciencedirect.com
ScienceDirect
Trans. Nonferrous Met. Soc. China 35(2025) 2484−2499
Transactions of Nonferrous Metals Society of China
www.tnmsc.cn

Interfacial structure and mechanical properties of Al/Cu laminated composite fabricated by hot press sintering

Kai-qiang SHEN[1,2], Liang CHEN[1,2], Li-hua QIAN[1,2], Biao-hua QUE[1,2], Cun-sheng ZHANG[1,2]

1. Key Laboratory for Liquid−Solid Structural Evolution and Processing of Materials (Ministry of Education), Shandong University, Jinan 250061, China;
2. School of Materials Science and Engineering, Shandong University, Jinan 250061, China

Received 5 December 2023; accepted 1 July 2024

Abstract: Al/Cu laminate composite was fabricated based on hot press sintering using Cu sheet and Al powders as raw materials. The effects of sintering parameters on interfacial structure and mechanical properties were investigated. The results revealed that a uniform Al/Cu interface with excellent bonding quality was achieved. The thickness of intermetallic compounds (IMCs) reached 33.88 μm after sintering at 620 °C for 2 h, whereas it was only 14.88 μm when sintered at 600 °C for 1 h. AlCu phase was developed through the reaction between Al_4Cu_9 and Al_2Cu with prolonging sintering time, and an amorphous oxide strip formed at AlCu/Al_4Cu_9 interface. Both the grain morphology and interfacial structure affected the tensile strength of Al/Cu laminate, whereas the mode of tensile fracture strongly relied on the interfacial bonding strength. The highest tensile strength of 151.1 MPa and bonding strength of 93.7 MPa were achieved after sintering at 600 °C for 1 h.

Key words: Al/Cu laminated composite; interface; intermetallic compounds; bonding strength; mechanical properties

1 Introduction

Cu alloys have superior thermal/electrical conductivity, good ductility, and high strength. Since the lightweight has become an important trend in industry, the high density of Cu alloys is considered as a major problem. As the most important lightweight metallic materials, Al alloys have the advantages of excellent formability and good corrosion resistance [1], and their thermal/electrical conductivity is only slightly lower than that of Cu alloys. Hence, fabricating Al/Cu laminated composite to combine the advantages of both alloys has attracted much attention [2−4]. Till now, Al/Cu laminate has been applied in the fields of conduction systems, batteries, and automotive industries [5].

In Al/Cu laminate, the interface between Al and Cu layers can be bonded under a condition of high temperature and deformation, and the final performance strongly depends on both the bonding quality and interfacial structure [6,7]. In general, the metallurgical bonding is firstly realized between Al and Cu layers. Cu and Al atoms diffuse into their opposing matrixes, and a brittle intermetallic compounds (IMCs) layer forms at Al/Cu interface. The layer affects the bonding quality, interface strength, and overall mechanical properties of Al/Cu laminate. Based on the Al−Cu binary phase diagram, it is known that Al_4Cu_9, Al_2Cu_3, Al_3Cu_4, AlCu, and Al_2Cu phases are the possible IMCs. CHANG et al [8] reported that the IMCs layer at Al/Cu interface was composed of Al_2Cu, Al_4Cu_9 and AlCu. JIANG et al [9] calculated the apparent activation energies for the formation of Al_2Cu and

Corresponding author: Liang CHEN, Tel: +86-531-81696577, Fax: +86-531-88392811, E-mail: chenliang@sdu.edu.cn
https://doi.org/10.1016/S1003-6326(25)66828-2

Al_4Cu_9 as 0.78 and 0.83 eV in Cu-rich area, respectively, which were smaller than the normal values, suggesting that the reactions at Al/Cu interface were controlled by interfacial and grain boundary diffusion. ZHANG et al [10] reported that the growth of IMCs layers in Al/Cu laminate conformed to a diffusion-controlled kinetic mechanism. XU et al [11] found that the high magnetic field increased the growth activation energy of IMCs layers. BESSON et al [12] reported that Al_4Cu_9 formed through non-thermally activated mechanisms in Al−25at.%Cu mixture produced by mechanical alloying. The above open literatures [6−12] indicate that in the metallurgical bonding process of Al/Cu interface, the types and formation order of the IMCs are different and depend on both the formation energy and formation mechanism.

Till now, multiple methods have been developed to prepare Al/Cu laminate, such as the friction stir welding [13], electron beam welding [14], continuous casting [15], and accumulative roll bonding (ARB) [16−22]. MAO et al [13] prepared dissimilar 6061-T6 Al and T2 pure Cu joints by submerged friction stir welding (SFSW), and the thin and uniform IMCs layer was achieved. WANG et al [15] carried out the horizontal continuous composite casting to prepare Al/Cu laminate with a thickness of 2 mm, and concluded that the increase of first-pass reduction and rolling temperature was beneficial to the bonding strength. RAHMATABADI et al [22] produced the ultrafine grained Al5052/Cu composite by ARB, and found that the plane stress fracture toughness of Al5052/Cu composite increased with increasing number of ARB cycles. MAO et al [23] enhanced the interfacial bonding degree of Al/Cu laminate and controlled the thickness of IMCs layer within 550 nm by rolling and subsequent annealing at 250 °C. The above studies indicate that controlling the thickness and composition of IMCs layer plays an important role in the bonding strength and mechanical properties of Al/Cu laminate [24−29].

This study aimed to assess the practicability of producing Al/Cu laminate through the vacuum hot press sintering method. Unlike the traditional sheet/sheet stack method, the proposed hot press sintering process enabled Al powders to establish a closer contact with the Cu sheet. This configuration could enhance the bonding quality of Al/Cu interface and help to mitigate the thermal stress between layers, and the vacuum atmosphere further prevented the impurities and oxides at the interface. Moreover, the effects of sintering factors on the microstructure, interfacial structure, and mechanical properties of Al/Cu laminate were clarified.

2 Experimental

2.1 Materials and experimental procedures

Pure Al powders and T2 Cu sheet were used as the raw materials for Al/Cu laminate. Al powders (Changsha TIJO Metal Material Co., Ltd., China) had spherical shape and the size of 21−23 μm. The purity of Al powders was greater than 99.8%. T2 Cu sheet (Shanghai Zhuoshun Metal Products Co., Ltd., China) had a diameter of 55 mm and a thickness of 1 mm.

Figure 1 schematically shows the preparation procedures of Al/Cu laminate. In order to refine Al powders and improve their sintering performance, the ball milling was conducted prior to hot press sintering in an internal argon atmosphere. The mass ratio of grinding balls to powders, rotation speed, and rotation time were 5∶1, 300 r/min, and 2 h, respectively. In order to remove the oxides and impurities on the surface, the T2 Cu sheet was put into a 15 vol.% HCl solution for about 10 s. Then, the ultrasonic cleaning was carried out in an ethanol solution for 15 min. After that, Al powders and Cu sheets were alternately stacked inside a graphite

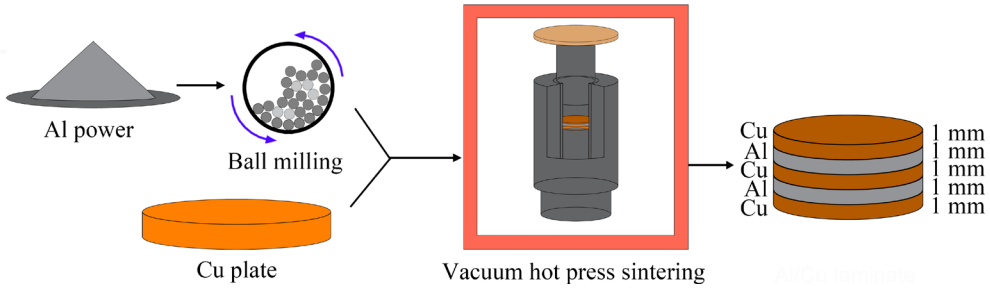

Fig. 1 Schematic illustration of fabrication process of Al/Cu laminate

mold to construct Al/Cu laminate with 3 Cu layers and 2 Al layers. The hot press sintering furnace (ZT−40−21Y, Chenhua, China) was used to perform sintering, during which the heating rate, applied pressure, and vacuum degree were 10 °C/min, 30 MPa, and 8×10^{-4} Pa, respectively. The sintered sample with a cylindrical shape had a diameter of 55 mm and a thickness of 5 mm (1 mm for each Al or Cu layer). Various sintering temperatures (600 and 620 °C) and holding time (1, 2, and 4 h) were attempted. Accordingly, the samples were abbreviated as 600-1, 600-2, 600-4, and 620-2, respectively. The former number indicated the sintering temperature and the latter number indicated the holding time.

2.2 Microstructure characterization and mechanical properties tests

The scanning electron microscope (SEM, JSM−7800F, JEOL, Japan) was adopted to observe the morphology of Al/Cu interface, and the energy dispersive spectrometer (EDS, JSM−7800F, JEOL, Japan) was used to analyze the behavior of elemental diffusion. The SEM and EDS samples were mechanically polished to have a mirror surface. The grain structure was examined by electron backscatter diffraction (EBSD, JSM−7800F, JEOL, Japan), and the sample was prepared by diamond polishing and subsequent argon ion polishing (AIP). The scanning area was around 250 μm × 150 μm, and the scanning step was set to be 0.3 μm. In order to determine the compositions of IMCs and the lattice structure at Al/Cu interface, the transmission electron microscopy (TEM, Talos F200X, FEI, USA) analysis was conducted, and the TEM sample was prepared based on focused ion beam (FIB) technique.

The microhardness across Al matrix, Al/Cu interface, and Cu matrix was measured based on nano-indentation system (Hysitron TI980, BRUKER, USA) using a triangular Berkovich diamond indenter. Moreover, the tensile test was conducted on a universal testing machine (E45.105, MTS, USA) at ambient temperature, and the sample had a gauge length of 14 mm. The digital image correlation (DIC, Const, XTDIC, China) system was equipped to in-situ observe the deformation and fracture behavior during the tensile test. The three-point bending test was used to evaluate the bonding strength between Al and Cu layers. The sample for bending test had a V-notch with a depth of 0.5 mm, and its dimensions were around 40 mm × 6 mm × 5 mm.

3 Results

3.1 Microstructure and Al/Cu interfacial structure

Figure 2 shows the SEM images of the Al/Cu

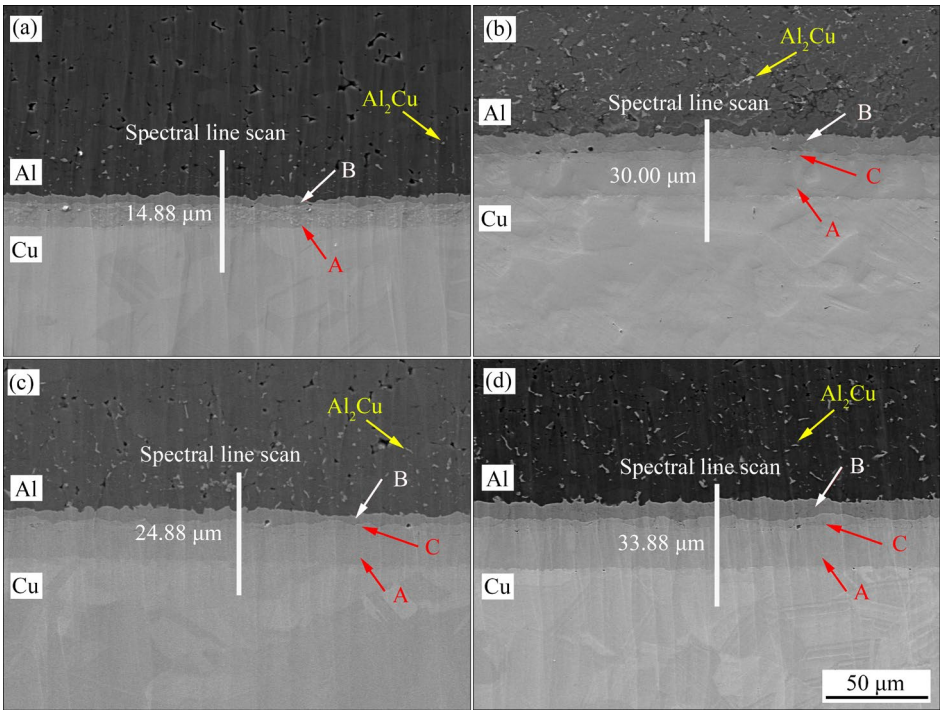

Fig. 2 SEM images across Al/Cu interfaces of 600-1 (a), 600-2 (b), 600-4 (c), and 620-2 (d) samples

laminates at various sintering temperatures and time. As is seen, good metallurgical bonding is achieved at all Al/Cu interfaces, and no obvious cracks or voids can be observed. This indicates that using the hot press sintering method developed in this study can fabricate the Al/Cu laminates with high bonding quality. In 600-1 sample, two different IMCs layers are observed at Al/Cu interface and they distribute in the form of unsmooth strips, as shown in Fig. 2(a). The IMCs layer close to Cu layer is labeled as A, and that close to Al layer is labeled as B. In 600-2, 620-2, and 600-4 samples, three IMCs layers are observed at Al/Cu interface, as shown in Figs. 2(b−d). The new layer formed between A and B is labeled as C. Moreover, it is obviously seen that large amounts of tiny particles distribute in Al layers, as marked by the yellow arrows in Fig. 2. According to EDS results, the Al/Cu atom ratio of these particles is close to 2:1, indicating that they should be Al_2Cu phase. The total thickness of IMCs layer was measured, and the average value is marked in Fig. 2. When the sintering temperature is 600 °C, the thickness of IMCs layer greatly increases from 14.88 to 30.00 μm as the sintering time increases from 1 to 2 h. It is interesting that the thickness decreases to 24.88 μm with a sintering time of 4 h. The reason will be discussed in the latter section. Comparing Fig. 2(b) with Fig. 2(d), it is clear that high sintering temperature causes an increase in the thickness of IMCs layer to 33.88 μm.

EDS line scanning was performed across the Al/Cu interfaces, and the results are plotted in Fig. 3. It is seen that a certain diffusion depth exists between Al and Cu layers. Overall, the longer the sintering time or the higher the temperature is, the more deeply the atoms diffuse into each other. The content of Cu in Al layer fluctuates in some regions, corresponding to the tiny Al_2Cu particles distributed in Al layer. It has been mentioned that different IMCs layers (A, B, and C) formed at Al/Cu interface. In order to preliminarily determine the types of IMCs, the spectral point analysis was performed and the results are listed in Table 1. It is found that the average Al/Cu atom ratios in the A, B, and C layers are close to 1:2, 2:1, and 1:1, respectively. Hence, combined the EDS results and the previous studies, the IMCs of the A, B, and C layers are determined as Al_4Cu_9, Al_2Cu, and AlCu, respectively [30].

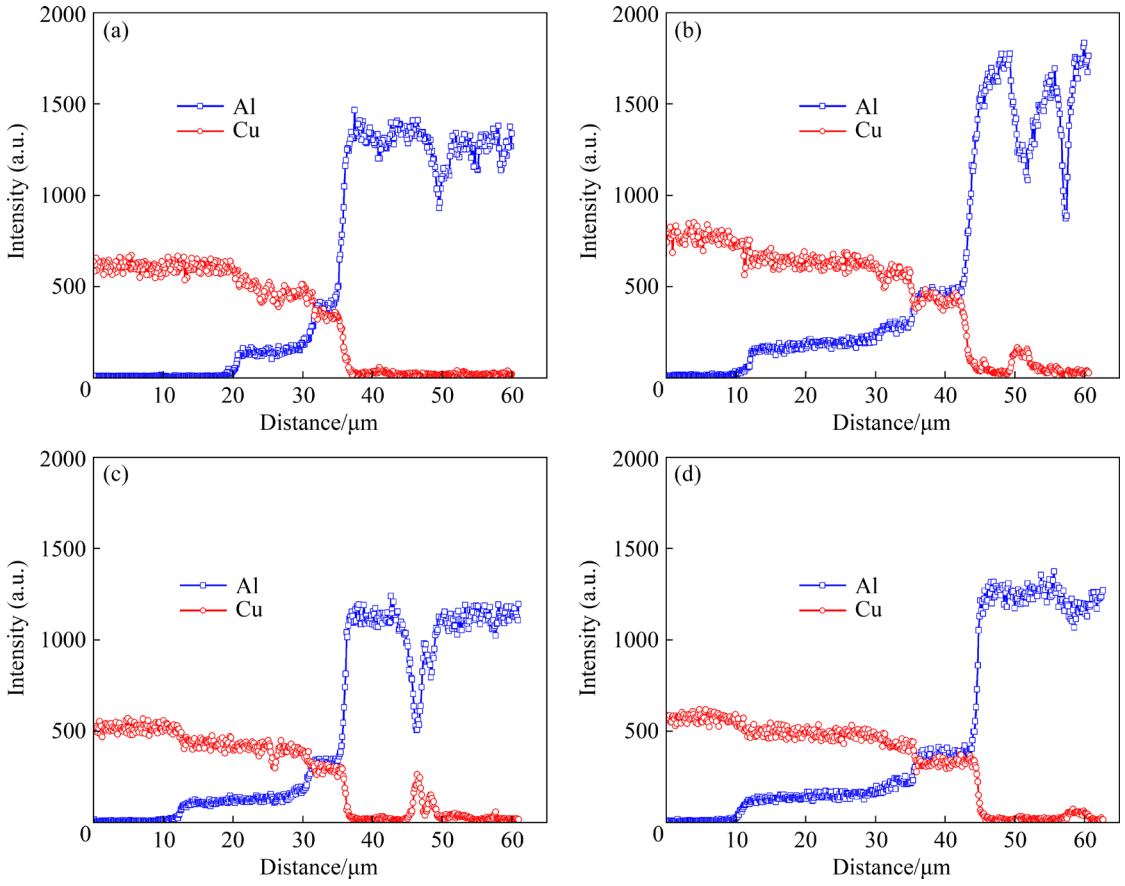

Fig. 3 EDS line scanning results across Al/Cu interfaces of 600-1 (a), 600-2 (b), 600-4 (c), and 620-2 (d) samples

Table 1 Spectral point analysis results of IMCs layers in different samples

Sample	Layer	Al content/at.%	Cu content/at.%
600-1	A	35.0	65.0
	B	62.5	37.5
	C	–	–
600-2	A	38.57	61.43
	B	66.3	33.7
	C	50.7	49.3
600-4	A	34.06	65.94
	B	65.2	34.8
	C	54.0	46.0
620-2	A	38.3	61.7
	B	66.2	33.8
	C	50.8	49.2

In order to further determine the types of IMCs and conduct a nanoscale analysis on the interfaces between different IMCs layers, 600-4 sample was selected for TEM observation. The bright field (BF) images shown in Figs. 4(a, b) reveal three distinct IMCs layers and corresponding two layer-to-layer interfaces. Figures 4(c, d) depict the magnified BF images of the Al_4Cu_9/AlCu and AlCu/Al_2Cu interfaces, respectively. As is seen, a thin bright strip exists at Al_4Cu_9/AlCu interface. However, the connection at Al_2Cu/AlCu interface is tight, and the transition is smooth and flat. Figure 4(f) shows the EDS results of the O element distribution at AlCu/Al_4Cu_9 interface. It is clear that the O element segregation area agrees well with the position of the bright strip shown in Fig. 4(c), confirming that the

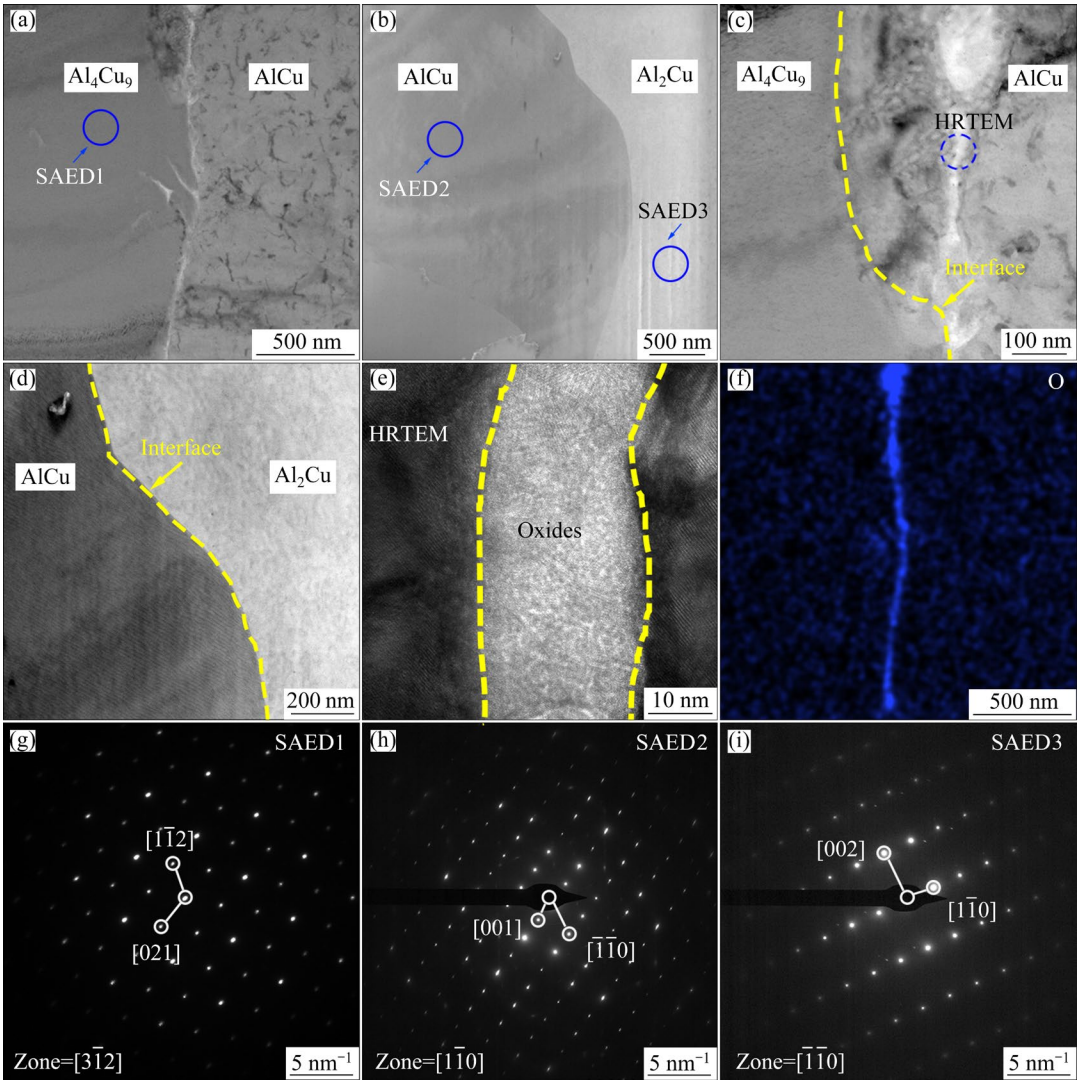

Fig. 4 TEM analysis results of 600-4 sample: (a) BF image showing Al_4Cu_9, AlCu, and Al_4Cu_9/AlCu interface; (b) BF image showing AlCu, Al_2Cu, and AlCu/Al_2Cu interface, (c, d) Enlarged BF images showing Al_4Cu_9/AlCu and AlCu/Al_2Cu interfaces, respectively; (e) HRTEM image; (f) O distribution corresponding to oxide strip at Al_4Cu_9/AlCu interface; (g, h, i) SAED patterns of Zones SAED1, SAED2, and SAED3, respectively

strip should be composed of oxides. Figure 4(e) shows the high-resolution TEM (HRTEM) image of the dotted circle marked in Fig. 4(c). As is seen, the oxide strip presents an amorphous state, and there is a transition connection with the phase intermediate. Figures 4(g−i) show the selected area electron diffraction (SAED) patterns of Zones SAED1, SAED2, and SAED3 marked in Figs. 4(a, b). The body-centered tetragonal structure, face-centered cubic simple dot matrix, and monoclinic C bottom-centered dot matrix are identified in SAED1, SAED2, and SAED3, which correspond to Al_2Cu, Al_4Cu_9, and AlCu phases, respectively. These facts further prove the conclusions drawn from the EDS results presented in Table 1.

Figures 5(a−c) show the HRTEM images and inverse fast Fourier transform (IFFT) maps of Al_4Cu_9, AlCu, and Al_2Cu, respectively. It is clear that the distortion degree of lattice structure varies significantly in different phases. The lattice stripe images are given in Figs. 5(d−f) by performing IFFT on the red boxed areas indicated in Figs. 5(a−c). It is determined that the lattice orientations of Al_4Cu_9, AlCu, and Al_2Cu are (112) with a lattice spacing of d=0.360 nm, (001) with a lattice spacing of d=0.562 nm, and (110) with a lattice spacing of d=0.462 nm, respectively. As shown in Fig. 5(d), a severe lattice distortion exists in Al_4Cu_9 phase, and lots of edge-type dislocations indicated by symbol “T” as well as the mixed

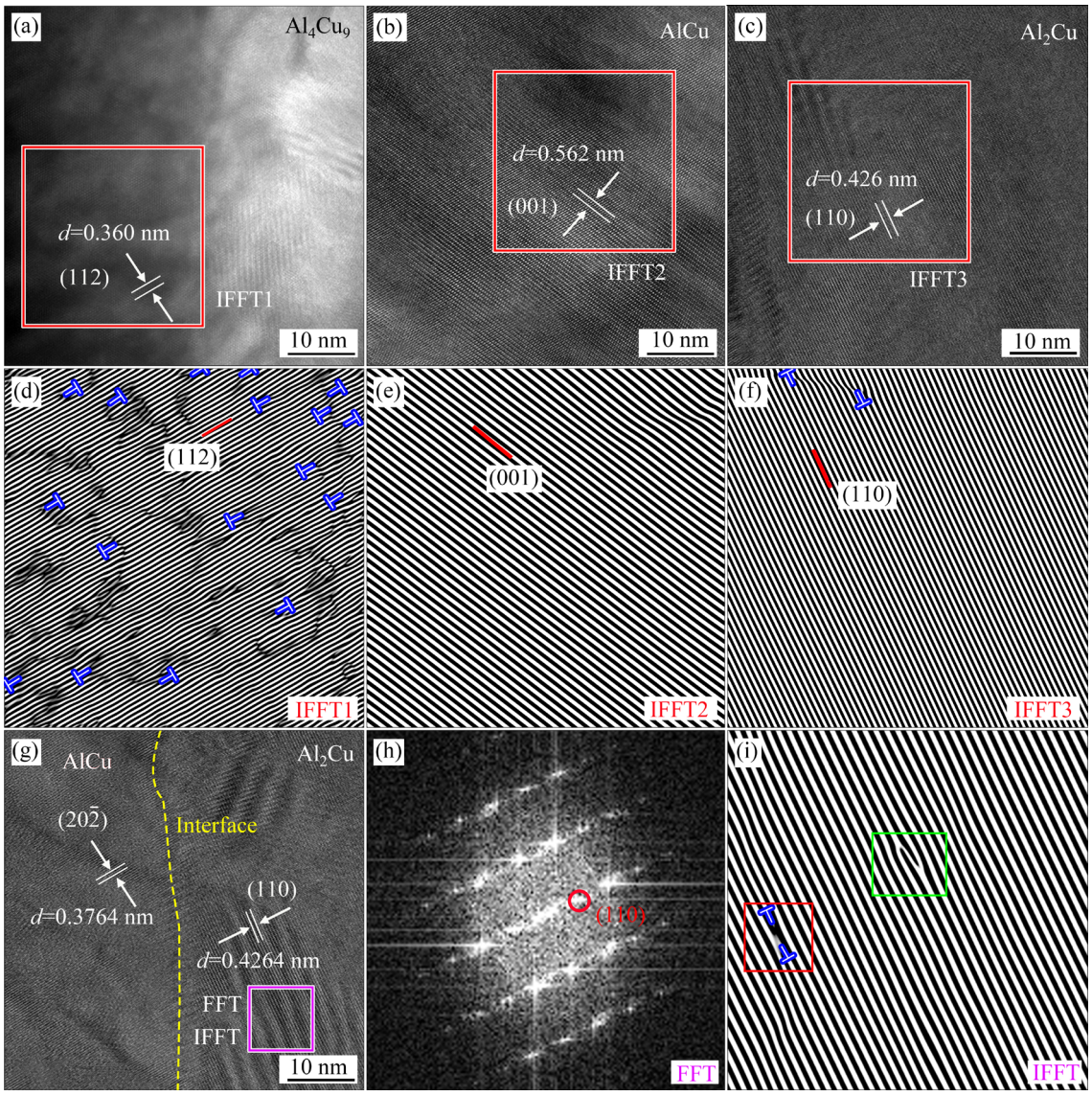

Fig. 5 Nanoscale analysis results of Al_4Cu_9, AlCu, Al_2Cu and Al_2Cu/AlCu interface: HRTEM images of Al_4Cu_9 (a), AlCu (b), and Al_2Cu (c); IFFT images of Al_4Cu_9 (d), AlCu (e), and Al_2Cu (f); (g) HRTEM image of AlCu/Al_2Cu interface; FFT (h) and IFFT (i) images of purple boxed region indicated in (g)

dislocations appear. Figure 5(e) shows that only partial lattice distortion with no obvious dislocations exists in AlCu. Figure 5(f) reveals that there are obvious lattice distortions and a small number of edge-type dislocations in Al_2Cu. Both Al_2Cu and Al_4Cu_9 initially form as solid solutions, and then the IMCs eventually form. The entry of dissimilar metal atoms into the matrix lattice can induce distortion, and thus the lattice distortion of Al_2Cu and Al_4Cu_9 is severer than that of AlCu. Figure 5(g) depicts the HRTEM image of AlCu/Al_2Cu interface. The lattice structures of AlCu and Al_2Cu are different, and there is an interfacial transition region between them with severe lattice distortion and dislocation cluster. The orientation of Al_2Cu side is (110) with a lattice spacing of d=0.4264 nm, and that of AlCu side is $(20\bar{2})$ with a lattice spacing of d=0.3764 nm, and there is a certain phase difference between them with an angle of about 15°. Moreover, Al_2Cu exhibits some stacking faults near the interface, as indicated by the purple box in Fig. 5(g). The fast Fourier transform (FFT) is performed on the purple boxed area, and the result is displayed in Fig. 5(h). As is seen, the diffraction spot along the direction of (110) crystal plane shows as a straight line with obvious stacking fault features. The IFFT result of the purple boxed area is shown in Fig. 5(i). The lattice stripe in the green box indicates the existence of stacking fault and the lattice region marked by two opposite symbol “T” in the red box is a characteristic of the existence of dislocation ring. This indicates that there is a role of pressure deformation mechanism in the formation of Al_2Cu.

Figure 6 displays the inverse pole figures (IPFs) and phase images of Al and Cu obtained from EBSD analysis. As is seen from the IPFs, in all samples, no obvious selective orientation is observed, and significant differences can be observed in the grain morphology of each layer. As is seen from the phase images, the grains of Al_4Cu_9 show obvious polygonal shapes, and their grain size is much larger than that of AlCu and Al_2Cu. It is noted that some dispersed Al_2Cu particles are distributed at the grain boundaries of Al layer, which agrees with the SEM results shown in Fig. 2. This indicates the precipitation of the Al_2Cu phase, and the reasons are explained as follows. The Cu concentration gradually decreases with increasing distance from Al/Cu interface, and it is no longer sufficient to form a uniform Al_2Cu layer. However, the high sintering temperature can provide a driving force to make Cu atoms aggregate at the grain boundaries. Hence, the relatively high Cu concentration at grain boundaries can reach the condition of forming Al_2Cu, and the dispersed Al_2Cu particles precipitate.

Figure 7 shows the pole figures of Al and Cu layers in different samples. As is seen, the texture strength of Al layer is relatively low and shows a uniform distribution, and the influence of sintering parameters on the texture strength and distribution is not significant. However, the Cu layer exhibits significantly higher texture strength compared to Al layer. As the sintering temperature increases, the texture strength of Cu layer increases, and the texture distribution becomes more uniform. With the extension of the sintering time from 1 to 2 h, the texture of Cu layer is deflected and its strength slightly increases. However, when the sintering time is extended to 4 h, the texture strength of Cu layer decreases with a uniform distribution.

Figure 8 shows the grain size distribution and average grain size of different IMCs. As is seen, Cu layer consists of many large grains and few small grains, while the grains in Al layer are more uniform in size and much smaller than those in Cu layer. At the sintering temperature of 600 °C, the average size of Cu grains slightly decreases with increasing the time from 1 to 4 h, indicating the occurrence of partial dynamic recrystallization. The grain size of Al layer is not sensitive to the sintering time, while it obviously increases by a high sintering temperature of 620 °C. The average grain size of Al_4Cu_9 is the largest, and that of AlCu is the smallest. With the extension of sintering time, the average grain sizes of Al_2Cu and AlCu phases show an increasing trend, while that of Al_4Cu_9 firstly increases and then decreases. Since Al layer was fabricated from the loose Al powders, the diffusion velocity of Al atoms into Cu layer is much faster than that of Cu atoms into Al layer. As a result, the solid solution firstly forms in the Cu layer close to Al/Cu interface. When Al concentration reaches a certain degree, Al_4Cu_9 begins to form under the condition of high temperature, and it tends to gradually grow deeper into Cu layer due to the concentration gradient [8]. With further increase of sintering time, the recrystallization of Al_4Cu_9 takes place, thereby reducing the grain size.

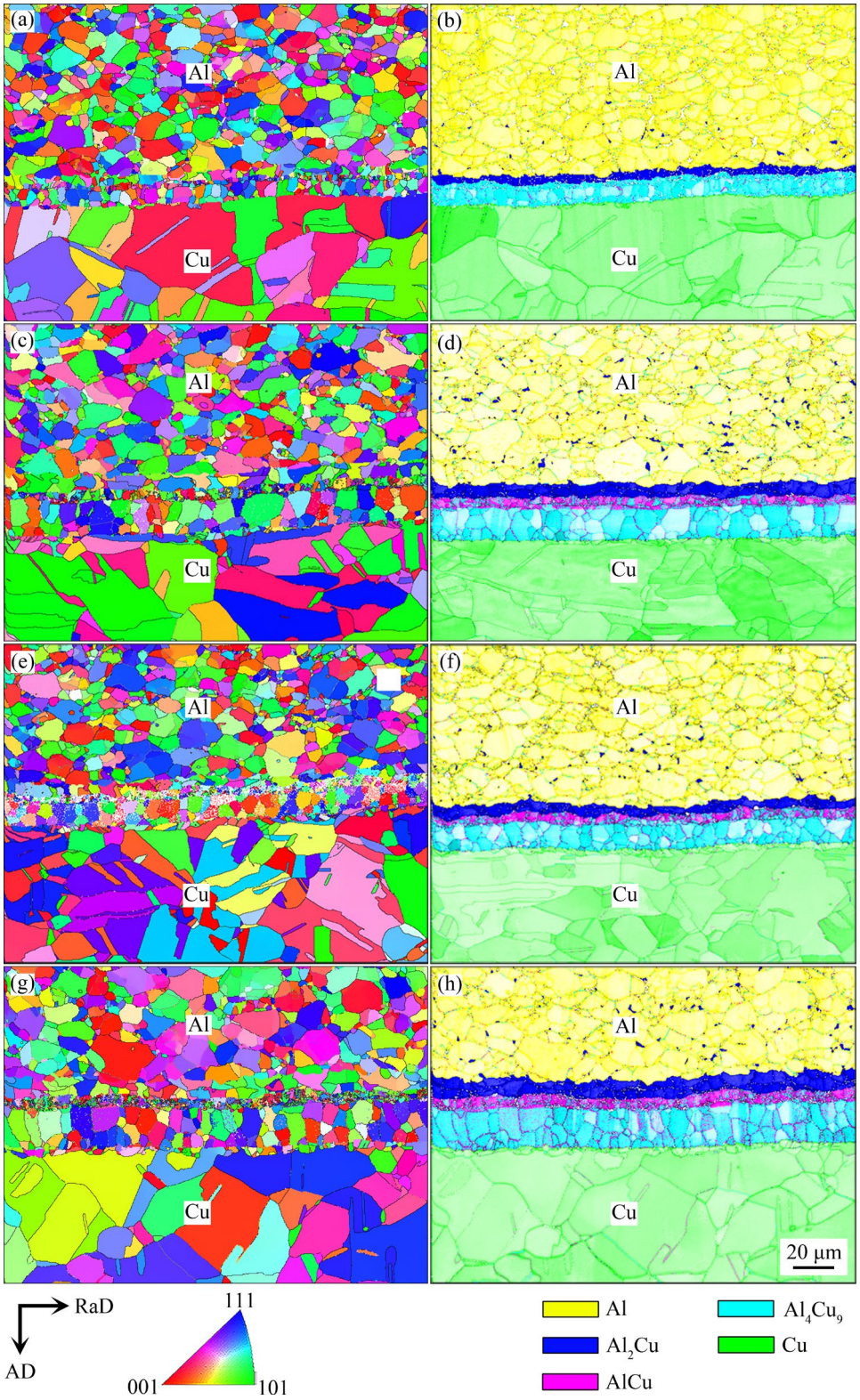

Fig. 6 EBSD results of IPFs (a, c, e, g) and phase images (b, d, f, h) of 600-1 (a, b), 600-2 (c, d), 600-4 (e, f), and 620-2 (g, h) samples

3.2 Mechanical properties

Figure 9(a) indicates the bonding strength obtained from the three-point bending tests of the Al/Cu laminates with different sintering parameters. As is seen, the bonding strengths of 600-1 and 600-4 samples are 93.7 and 93.2 MPa, respectively, indicating a good interfacial bonding. However, the bonding strength of 600-2 and 620-2 are relatively

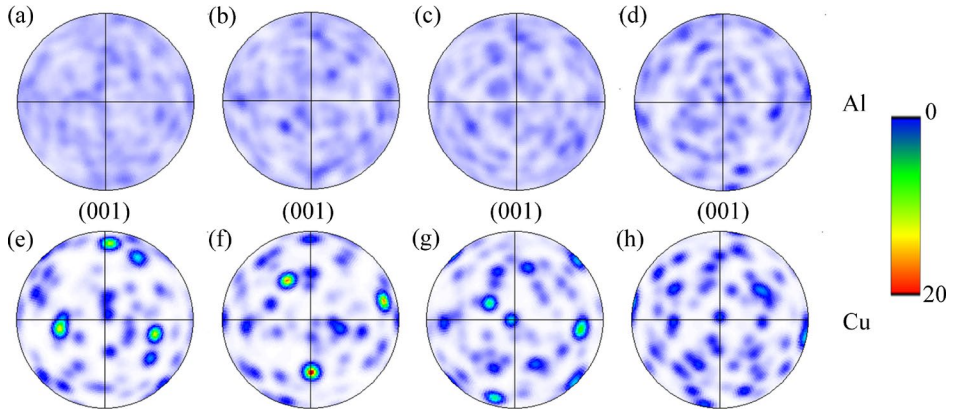

Fig. 7 Pole figures of Al (a−d) and Cu (e−h) layers in 600-1 (a, e), 600-2 (b, f), 600-4 (c, g), and 620-2 (d, h) samples

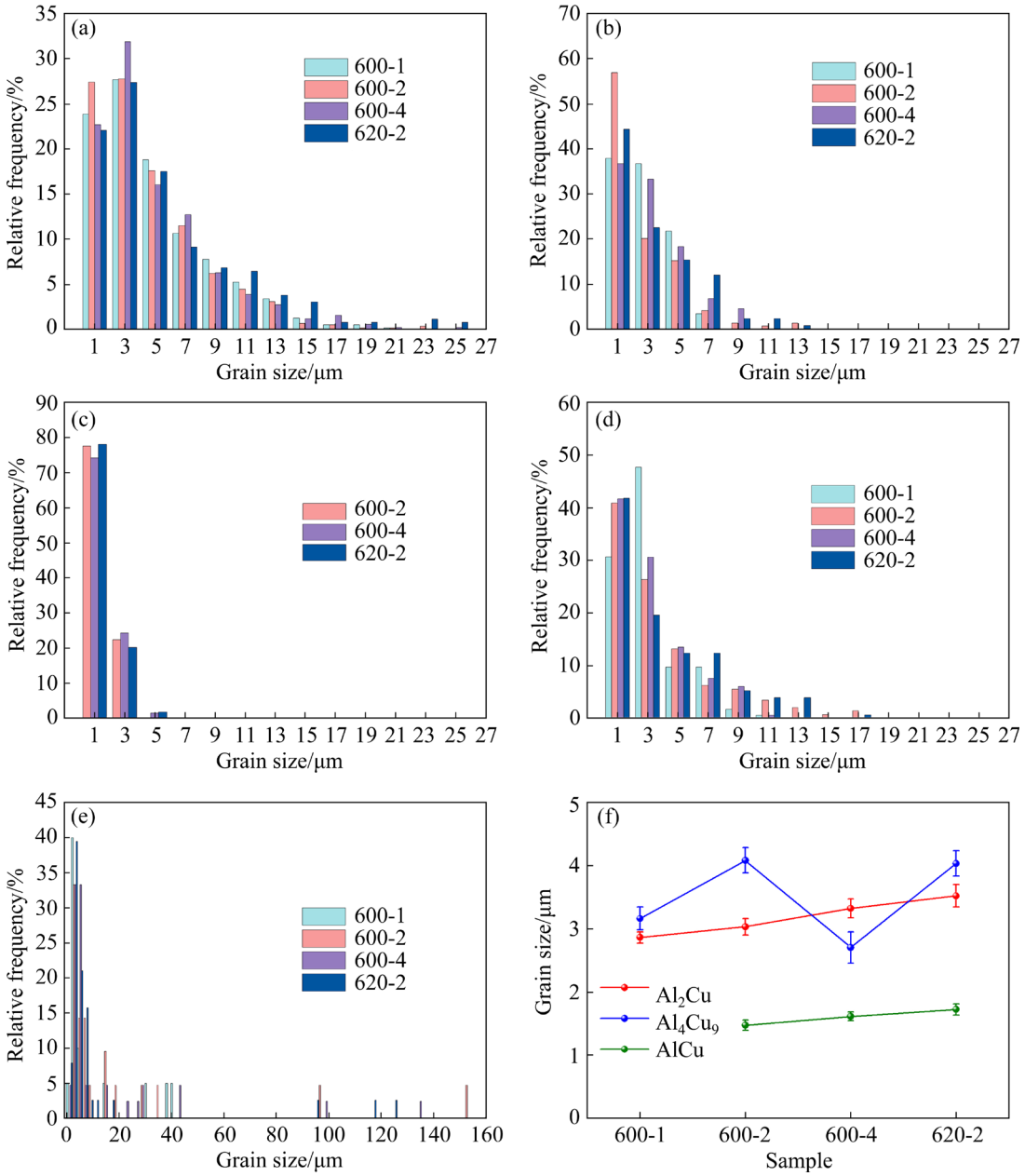

Fig. 8 Grain size distribution of Al (a), Al_2Cu (b), AlCu (c), Al_4Cu_9 (d) and Cu (e), and average grain size statistics of IMCs (f)

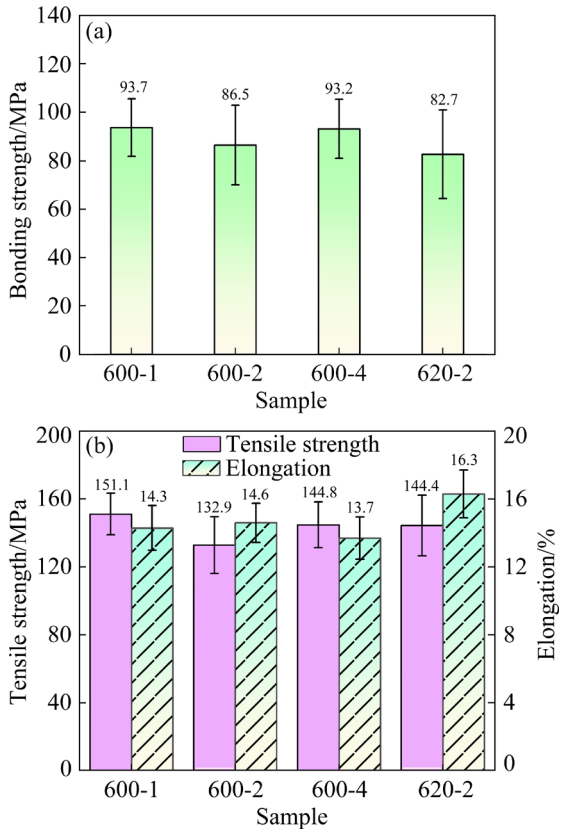

Fig. 9 Mechanical test results of Al/Cu laminates: (a) Bonding strength; (b) Tensile strength and elongation

much lower, and the lowest value of 82.7 MPa appears in 620-2. Figure 9(b) shows the tensile strength results. As is seen, the tensile strength shows a tendency of decreasing and then increasing with the extension of the sintering time. Comparing the tensile strength of 600-1 and 600-2, it gradually decreases from 151.1 to 132.9 MPa. When the sintering time is extended to 4 h, the tensile strength gradually increases to 144.8 MPa. As the sintering temperature is raised from 600 to 620 °C with the same sintering time of 2 h, the tensile strength increases to 144.4 MPa, indicating an increasing trend with the increase of sintering temperature.

The 600-1 and 600-4 samples were selected to perform the nano-indentation test, and the load−displacement curves and the average hardness of different IMCs and matrix are plotted in Fig. 10. As is seen, the micromechanical properties of IMCs layer differ significantly from the matrix. Overall, the hardness of IMCs is much higher than that of Al or Cu matrix, and Al_4Cu_9 owns the highest hardness of greater than 10.3 GPa. During the plastic deformation process, the stress easily concentrates at Al/Cu interface and the deformation between the grains is delayed, which may interrupt the deformation coordination and promote the generation and extension of cracks. Hence, the cracks are generated and extended mainly in the brittle IMCs layer. In addition, the nanoscale oxide bands are observed in the IMCs layer of 600-4. These oxide bands can not only hinder the diffusion of Al and Cu atoms, but also increase the density of crystal defects and impede the dislocation motion, which may result in the severe dislocation-interface interactions and a certain degree of synergistic strengthening effect [31].

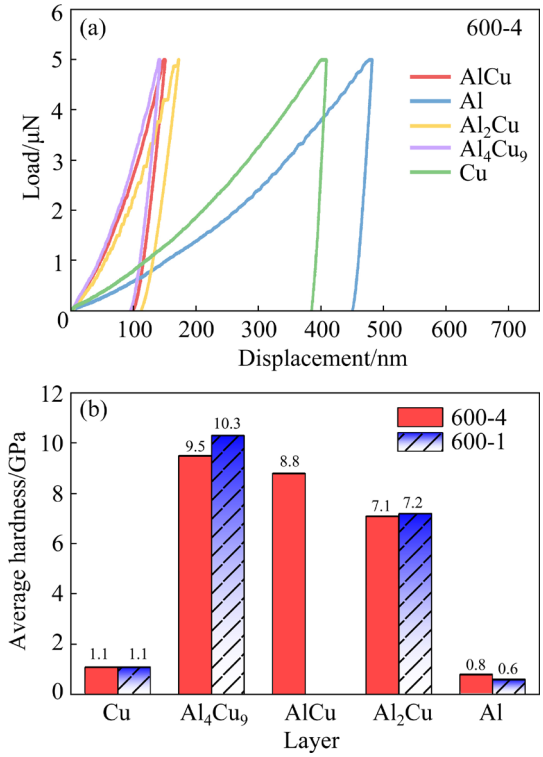

Fig. 10 Nano-indentation results of 600-1 and 600-4 samples: (a) Local load−displacement curves; (b) Average hardness

4 Discussion

4.1 Diffusion pattern across Al/Cu interface

As aforementioned, the thickness of IMCs layer firstly increases and then decreases with the extension of the sintering time. It is an unusual phenomenon which is contradictory to the conventional theory. It is widely accepted that the IMCs thickness keeps increasing with the extension of sintering time [10,32]. In hot press sintering process, the pressure is always applied on the sample to promote the sintering quality of Al layer and interfacial bonding of Al/Cu interface. The

mutual diffusion of Al and Cu atoms is the main factors increasing the thickness of IMCs, while the deformation and contraction of IMCs layer caused by pressure can reduce the thickness of IMCs [33]. At the early stage of sintering, the IMCs layer does not form or its thickness is thin. Hence, the resistance of Al and Cu atoms to diffuse across the IMCs layer is small, and the mutual diffusion rate of them is fast. Moreover, since the IMCs layer formed under pressure has high strength, the shrinkage effect of IMCs layer due to the applied pressure is small. Therefore, the thickness of IMCs greatly increases from 14.88 to 30.00 μm when the sintering time is extended from 1 to 2 h at 600 °C. As the thickness of IMCs increases, the resistance of Al and Cu atoms to diffuse across the IMCs layer becomes large, which can cause a decrease of the growth rate of IMCs layer. Moreover, with the extension of sintering time, the recrystallization continuously softens IMCs layer, and the applied pressure causes the shrinkage effect on IMCs layer. If the shrinkage effect is more significant than the expansion effect due to the atom diffusion, the thickness of IMCs layer tends to decrease. Hence, the thickness of IMCs layer decreases from 30.00 to 24.88 μm as the sintering time is extended from 2 to 4 h at 600 °C.

Figure 11 shows the kernel average misorientation (KAM) maps of 600-1, 600-2, 600-4, and 620-2 samples, and the KAM values. As is seen, at the sintering temperature of 600 °C, the KAM values of all IMCs decrease significantly as the sintering time

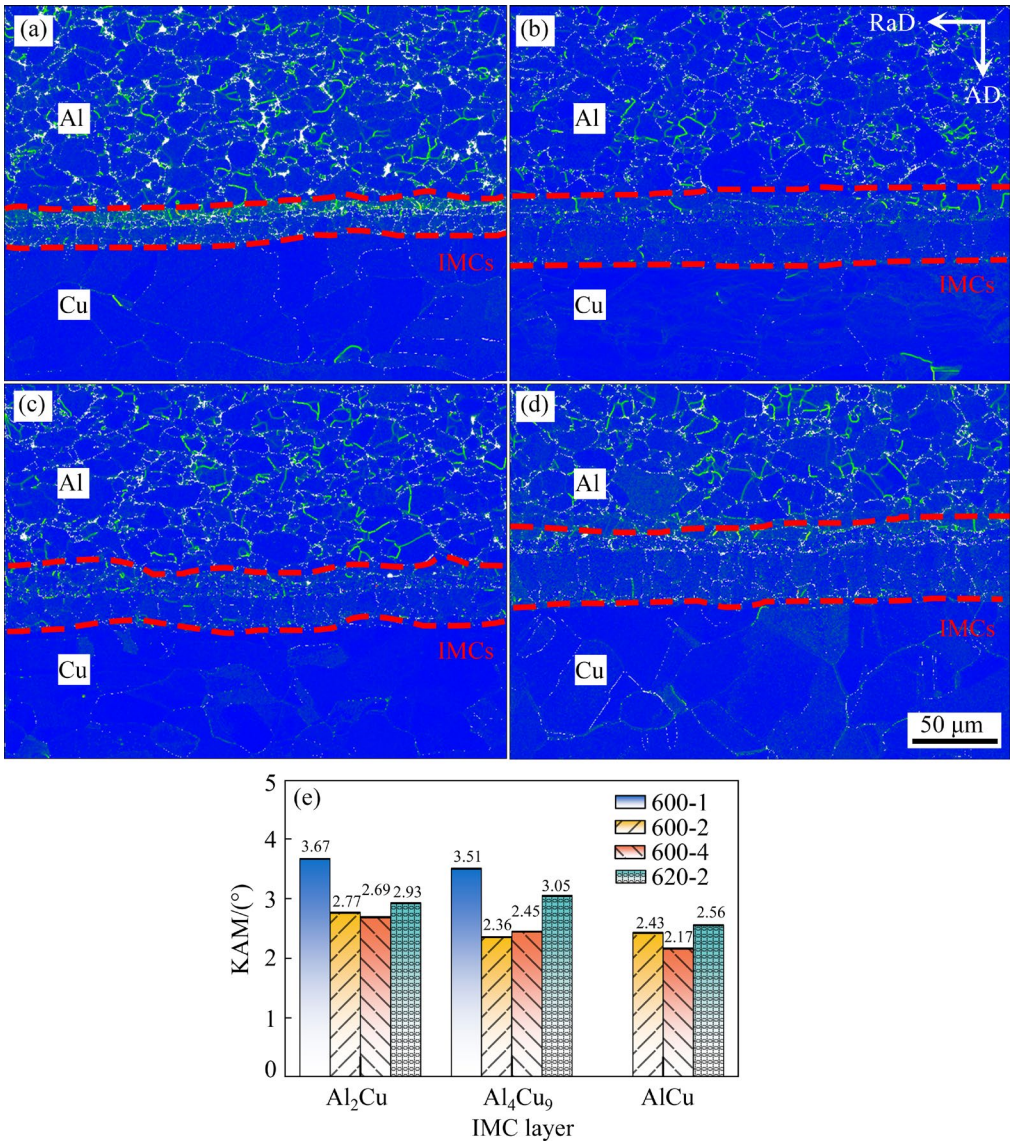

Fig. 11 KAM maps across Al/Cu interfaces of 600-1 (a), 600-2 (b), 600-4 (c) and 620-2 (d) samples, and statistics KAM values of different IMCs layers (e)

is extended from 1 to 2 h, while such decrease is very slight as the time is further extended to 4 h and the KAM value of Al_4Cu_9 even slightly increases. Comparing 600-2 and 600-4 samples, it is seen that the KAM values of all IMCs increase with increasing temperature. As is known, KAM value typically illustrates the stored strain energy between grains, and it is directly proportional to the dislocation density. In this study, the IMCs layer forms under the combined effects of temperature and pressure at the early stage of sintering, and the pressure plays a dominated role. Hence, the IMCs layer shows high KAM value and high dislocation density with the sintering time of 1 h. Then, the recrystallization is promoted by increasing sintering time, causing the elimination of dislocations and reduction of KAM values. When the sintering temperature increases from 600 to 620 °C, the thickness of IMCs layer changes slightly, while the variation of KAM value increases greatly. This indicates that the dislocation density accumulated by the deformation is more significant than the dislocation elimination caused by recrystallization at high sintering temperature.

4.2 Formation mechanism of IMCs layer

As aforementioned, Al_2Cu and Al_4Cu_9 are observed with the sintering time of 1 h, while as the time is greater than 2 h, the new phase of AlCu forms between Al_2Cu and Al_4Cu_9. These facts indicate that Al_2Cu and Al_4Cu_9 firstly form at Al/Cu interface during hot press sintering process, and then AlCu phase forms by the reaction of Al_2Cu and Al_4Cu_9 with the increase of sintering time. The formation mechanisms of different IMCs are schematically drawn in Fig. 12. BESSON et al [12] reported that Al_4Cu_9 could form in the Cu-rich zone during mechanical alloying and the formation of Al_4Cu_9 was driven by only a low thermal activation energy. It is seen from the IFFT image of Al_4Cu_9 in Fig. 5(d) that there are some edge-type dislocations and serious lattice distortion in Al_4Cu_9, which indicates that its formation is greatly affected by the applied pressure during hot press sintering. With the rise of temperature, Al and Cu atoms diffuse into each other. The Al-rich Al−Cu solid solution forms on the Al side of the interface, and Cu-rich Al−Cu solid solution forms on the Cu side. With the diffusion of Al atoms, when the temperature reaches a certain value, the formation condition of Al_4Cu_9 is satisfied, and it firstly nucleates in the Cu layer. After that, Al_4Cu_9 tends to gradually grow deeper into the Cu layer. Then, Al_2Cu nucleates in the Al−Cu solid solution on the Al side and grows with the diffusion of Cu atoms in the subsequent sintering process. The thermal activation energy required for the formation of Al_2Cu is higher than that of Al_4Cu_9. This means that higher temperature is required for the formation of Al_2Cu. AlCu is generated by a two-phase reaction after the formation of Al_2Cu and Al_4Cu_9 [9,34−36], and AlCu with a small thickness is distributed between Al_2Cu and Al_4Cu_9.

4.3 Effects of sintering parameters on mechanical properties

It is well known that the thicker the IMCs layer is, the more easily the cracks are generated and expanded at Al/Cu interface, and the lower the interfacial bonding strength is [24]. The tensile strength of Al/Cu laminate depends on the combined effects of Cu layer, Al layer, and IMCs layer. With the extension of the sintering time from 1 to 2 h, the degree of recrystallization of Cu rises, leading to the softening of Cu layer. Moreover, the thickness of IMCs layer increases, leading to the decrease of

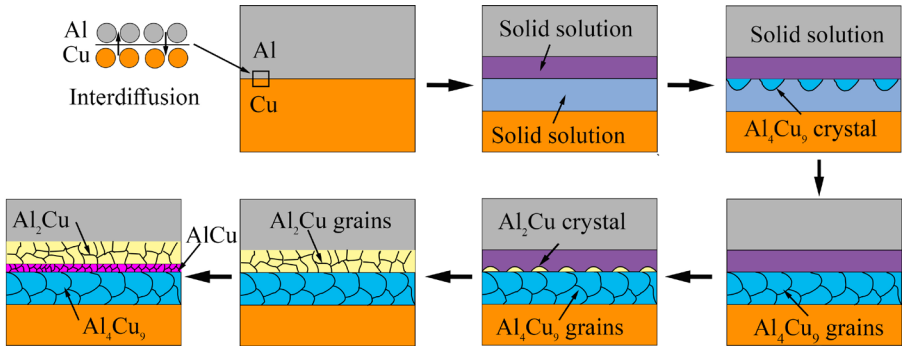

Fig. 12 Schematic diagram of formation of IMCs layer at Al/Cu interface during hot press sintering process

bonding strength of Al/Cu interface. These facts cause a decrease in the tensile strength of Al/Cu laminate. When the sintering time is extended to 4 h, the thickness of IMCs decreases, which is beneficial to the increase of bonding strength, and thus the tensile strength of 600-4 is improved. With the increase of sintering temperature to 620 °C, the sintering density and performance of Al layer are improved, and the tensile strength of Al layer increases. As a result, the tensile strength of 620-2 is higher than that of 600-2.

Figure 13 demonstrates two different fracture modes of Al/Cu laminate during the tensile test. Figure 13(a) shows the failure process of 600-1. Since the bonding strength of Al/Cu interface is higher than the tensile strength of Al layer, Al layer firstly fails and fractures during tension, while the separated Al layer is still combined with the Cu layer. In the subsequent tension, Al layer continues to deform along with the Cu layer until Cu layer fails because of the large differences in tensile strength and elongation between them. Finally, Al layer fractures into many small fragments, while the bonding of Al/Cu interface does not completely fail, and some Al fragments are still attached to the inner Cu layer. Figure 13(b) shows the failure process of 600-2 during the tensile test. The bonding strength of Al/Cu interface is lower than the tensile strength of Al layer, leading to lateral development and expansion of cracks in IMCs layer [23,37]. Consequently, failure firstly occurs at Al/Cu interface during tension. As a result, Al and Cu layers peel off from each other, and both of them deform separately under the action of tensile stress, showing an obvious delamination fracture. The final fracture morphology shows that the Al and Cu layers are fully separated and the fracture position is different. These results indicate that the bonding strength of Al/Cu interface determines the fracture mode of Al/Cu laminate. If the bonding strength is high, the failure firstly appears in Al layer, and Al/Cu interface is still in the bonding state. However, if the bonding strength is low, Al/Cu interface firstly fails at the early stage of tension, and then Al and Cu layers deform individually under the action of load. In order to obtain Al/Cu laminate with high mechanical performances, an IMCs layer with small thickness and low brittleness is required, and the sintering quality of Al layer is also important.

5 Conclusions

(1) No visible cracks or voids were detected at Al/Cu interface, and a stable IMCs layer consisting of Al_2Cu, Al_4Cu_9, and AlCu phases formed. The thickness of IMCs layer increased with the increase of sintering temperature, while it first increased and

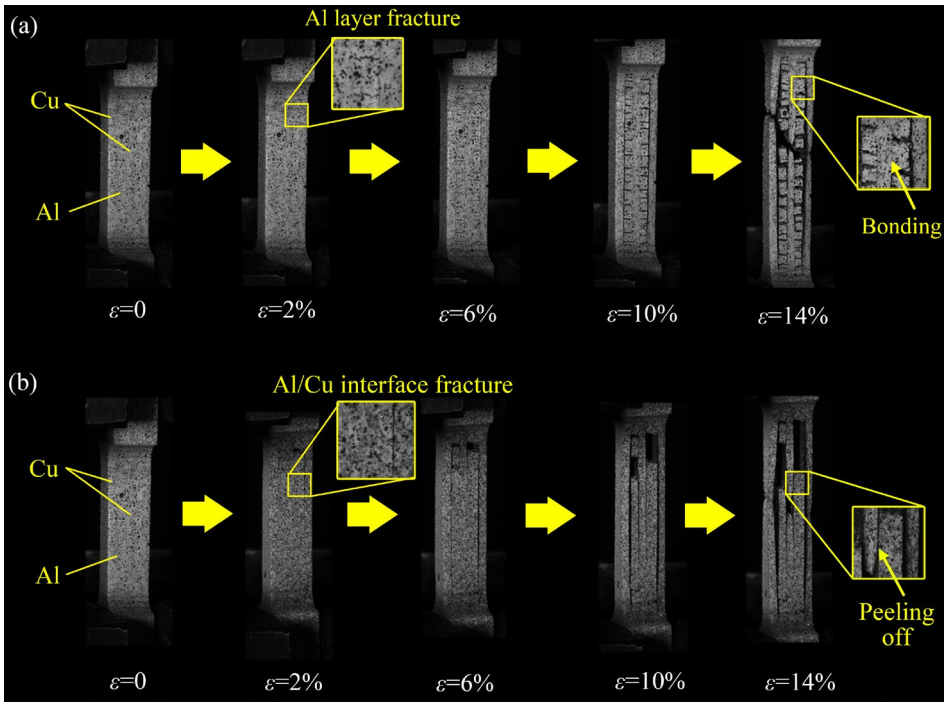

Fig. 13 Fracture processes during tensile tests of 600-1 (a) and 600-2 (b) samples

then decreased with the extension of time due to both the growth and shrinkage effects.

(2) Al_4Cu_9 first nucleated and grew at Al/Cu interface near the Cu side, followed by the nucleation of Al_2Cu near the Al side. Eventually, AlCu formed through the reaction between Al_4Cu_9 and Al_2Cu. Al_4Cu_9 exhibited a higher number of dislocations and severer lattice distortion compared to Al_2Cu and AlCu. The lattice distortion and atomic arrangement were significant at the interfaces of different IMCs phases, and an amorphous oxide strip was observed at AlCu/Al_4Cu_9 interface.

(3) The tensile strength showed a tendency to first decrease and then increase with the extension of sintering time, while it displayed an upward trend with the increase in temperature. The bonding strength of Al/Cu interface played a crucial role in determining the tensile fracture mode of Al/Cu laminate. When the bonding strength was high, Al layer tended to fracture into many small fragments, with some Al fragments still attached to the inner Cu layer. When the bonding strength was low, Al and Cu layers tended to completely separate.

CRediT authorship contribution statement

Kai-qiang SHEN: Conceptualization, Investigation, Methodology, Writing − Original draft; **Liang CHEN:** Conceptualization, Data curation, Funding acquisition, Investigation, Writing − Original draft; **Li-hua QIAN:** Data curation, Investigation; **Biao-hua QUE:** Investigation, Validation; **Cun-sheng ZHANG:** Writing − Review & editing.

Declaration of competing interest

The authors declare that they have no known competing financial interests or personal relationships that could have appeared to influence the work reported in this paper.

Acknowledgments

The authors would like to acknowledge the financial support from the National Natural Science Foundation of China (Nos. 51875317, 52222510), and Key Research and Development Program of Shandong Province, China (No. 2021ZLGX01).

References

[1] SHAO Hong-bang, HUANG Yuan-chun, WANG Yan-ling. Effect of ageing process on microstructure, corrosion behaviors and mechanical properties of Al−5.6Zn−1.6Mg−0.05Zr alloy [J]. Journal of Central South University, 2022, 29: 1029−1040.

[2] BERSKI S, DYJA H, MARANDA A, NOWACZEWSKI J, BANASZEK G. Analysis of quality of bimetallic rod after extrusion process [J]. Journal of Materials Processing Technology, 2006, 177: 582−586.

[3] MA Qiu-chen, SONG Cheng, ZHOU Jian-li, ZHANG Lin, JI Hong-jun. Dynamic Weld evolution during ultrasonic welding of Cu−Al joints [J]. Materials Science and Engineering: A, 2021, 823: 141724.

[4] WANG Chen, MA Li-nan, MA Xiao-guang, WANG Tao, JIANG Zheng-yi, HASAN M, ZHAO Jing-wei. Effect of annealing temperature on microstructure and tensile properties of copper/aluminum composite thin strip [J]. Transactions of Nonferrous Metals Society of China, 2023, 33: 701−713.

[5] TAYYEBI M, RAHMATABADI D, KARIMI A, ADHAMI M, HASHEMI R. Investigation of annealing treatment on the interfacial and mechanical properties of Al5052/Cu multilayered composites subjected to ARB process [J]. Journal of Alloys and Compounds, 2021, 871: 159513.

[6] LIU Yan-xiao, LIU Yuan-ming, WANG Zhen-hua, LIU Yan-ping, WANG Tao, HUAN Qing-xue. Stress analysis and microstructure evolution of Cu/Al composite plate during corrugated rolling [J]. Transactions of Nonferrous Metals Society of China, 2023, 33: 1460−1471.

[7] CHEN Xiao-ling, CHEN Zhi-qing, HU Bo, YAN Long, WANG Jing-ya, YING Tao, ZENG Xiao-qin. Strengthening behavior and thermal conductivity of Cu/Al composite with penetration architecture [J]. Transactions of Nonferrous Metals Society of China, 2024, 34: 236−245.

[8] CHANG Qing-hua, ZHANG Jun-yi, GAO Pei-kai, ZHANG Zheng, HUO Yi-qiang, XIE Jing-pei. Study on the phase structure of the interface zone of Cu−Al composite plate in cast-rolling state and different heat treatment temperatures based on EBSD [J]. Journal of Materials Research and Technology, 2023, 24: 1056−1069.

[9] JIANG Hai-gang, DAI Ji-yan, TONG Hai-yang, DING Bang-zhu, SONG Qing-hao, HU Zeng-quan. Interfacial reactions on annealing Cu/Al multilayer thin films [J]. Journal of Applied Physics, 1993, 74: 6165−6169.

[10] ZHANG Jian, WANG Bin-hao, CHEN Guo-hong, WANG Ruo-min, MIAO Chun-hui, ZHENG Zhi-xiang, TANG Wen-ming. Formation and growth of Cu−Al IMCs and their effect on electrical property of electroplated Cu/Al laminar composites [J]. Transactions of Nonferrous Metals Society of China, 2016, 26: 3283−3291.

[11] XU Bo, TONG Wei-ping, LIU Chun-zhong, ZHANG Hai-tao, ZUO Liang, HE Ji-cheng. Effect of high magnetic field on growth behavior of compound layers during reactive diffusion between solid Cu and liquid Al [J]. Journal of Materials Science & Technology, 2011, 27: 856−860.

[12] BESSON R, AVETTAND-FÈNOËL M N, THUINET L, KWON J, ADDAD A, ROUSSEL P, LEGRIS A. Mechanisms of formation of Al_4Cu_9 during mechanical alloying: An experimental study [J]. Acta Materialia, 2015,

87: 216−224.

[13] MAO Yue, QIN Ding-qiang, XIAO Xuan, WANG Xin-cheng, FU Li. Achievement of high-strength Al/Cu dissimilar joint during submerged friction stir welding and its regulation mechanism of intermetallic compounds layer [J]. Materials Science and Engineering: A, 2023, 865: 144164.

[14] XU Rong-zheng, LI Fu-shan, YUAN Chen-chen, ZHANG Yan, YAN Wan-di, ZHAO Xiao. Microstructure and phase constitution at the interface of double-sided electron beam welded Cu/Al clad metal sheet [J]. Materials Characterization, 2021, 182: 111517.

[15] WANG Jun, ZHAO Fan, XIE Guo-liang, HOU Yu-fei, WANG Rui, LIU Xin-hua. Rolling deformation behaviour and interface evaluation of Cu−Al bimetallic composite plates fabricated by horizontal continuous composite casting [J]. Journal of Materials Processing Technology, 2021, 298: 117296.

[16] LEE S M, IM Y D, MATSUMOTO R, UTSUNOMIYA H. Strength and electrical conductivity of Cu-Al alloy sheets by cryogenic high-speed rolling [J]. Materials Science and Engineering: A, 2021, 799: 139815.

[17] LI Sha, LUO Chao, LIU Zhi-dong, ZHAO Jing-wei, HAN Jian-chao, WANG Tao. Interface characteristics and mechanical behavior of Cu/Al clad plate produced by the corrugated rolling technique [J]. Journal of Manufacturing Processes, 2020, 60: 75−85.

[18] MAO Zhi-ping, XIE Jing-pei, WANG Ai-qin, WANG Wen-yan, LI Yan, MA Dou-qin. Interfacial microstructure and bonding strength of copper/aluminum clad sheets produced by horizontal twin-roll casting and annealing [J]. Materials Research Express, 2019, 6: 016505.

[19] MAHDAVIAN M M, KHODABANDEH A R, JAFARIAN H R, MIRDAMADI S. Evaluation of the macro/microstructure of Al/Cu/Sn/Ni multi-layered composite produced by accumulative-roll-bonding (ARB) and post-heat treatment [J]. Journal of Alloys and Compounds, 2022, 925: 166711.

[20] SHABANI A, TOROGHINEJAD M R, SHAFYEI A. Effect of post-rolling annealing treatment and thickness of nickel coating on the bond strength of Al−Cu strips in cold roll bonding process [J]. Materials & Design, 2012, 40: 212−220.

[21] XU Run-run, LIANG Ning-ning, ZHUANG Li-min, WEI Da-jie, ZHAO Yong-hao. Microstructure and mechanical behaviors of Al/Cu laminated composites fabricated by accumulative roll bonding and intermediate annealing [J]. Materials Science and Engineering: A, 2022, 832: 142510.

[22] RAHMATABADI D, MOHAMMADI B, HASHEMI R, SHOJAEE T. An experimental study of fracture toughness for nano/ultrafine grained Al5052/Cu multilayered composite processed by accumulative roll bonding [J]. Journal of Manufacturing Science and Engineering, 2018, 140: 101001.

[23] MAO Zhi-ping, XIE Jing-pei, WANG Ai-qin, WANG Wen-yan, MA Dou-qin, LIU Pei. Effects of annealing temperature on the interfacial microstructure and bonding strength of Cu/Al clad sheets produced by twin-roll casting and rolling [J]. Journal of Materials Processing Technology, 2020, 285: 116804.

[24] CHANG Yu-ling, CHEN Hong-sheng, ZHOU Jun, LIU Run-ai, NIE Hui-hui, WANG Wen-xian. Comprehensive study of hot deformation behavior and fracture mechanism of Al/Cu laminated composite [J]. Journal of Manufacturing Processes, 2023, 97: 48−61.

[25] CHENG Xian-ming, YANG Ke, WANG Jian, LV Wen-yue, ZHAO Jian-hua. Ultrasonic welding of Cu to Al cables bonding: Evolution of microstructure and mechanical properties [J]. Materials Characterization, 2023, 200: 112905.

[26] WU Yu-fan, GU Ji, SONG Min. Strength and ductility synergy in a laminated Cu/Cu−6Al alloy with graded interfacial region [J]. Journal of Alloys and Compounds, 2022, 921: 166102.

[27] LUO Jun-ting, ZHAO Shuang-jing, ZHANG Chun-xiang. Casting-cold extrusion of Al/Cu clad composite by copper tubes with different sketch sections [J]. Journal of Central South University, 2012, 19: 882−886.

[28] XU Wei, LIU Xiao-chun, LI Xiu-yan, LU Ke. Deformation induced grain boundary segregation in nanolaminated Al−Cu alloy [J]. Acta Materialia, 2020, 182: 207−214.

[29] ZHANG Yue-ling, YANG Chao, ZHOU Deng-shan, ZHE Yin, MENG Li-fang, ZHU Xin-kun, ZHANG De-liang. Effect of stacking fault energy on microstructural feature and back stress hardening in Cu−Al alloys subjected to surface mechanical attrition treatment [J]. Materials Science and Engineering: A, 2019, 740: 235−242.

[30] AO San-san, LI Chun-jie, ZHANG Wei, WU Man-peng, DAI Yu, CHEN Yao, LUO Zhen. Microstructure evolution and mechanical properties of Al/Cu ultrasonic spot welded joints during thermal processing [J]. Journal of Manufacturing Processes, 2019, 41: 307−314.

[31] YANG Wen-fan, GONG Ming-yu, YAO Jia-hao, WANG Jiang-wei, ZHENG Shi-jian, MA Xiu-liang. Hardening induced by dislocation core spreading at disordered interface in Cu/Nb multilayers [J]. Scripta Materialia, 2021, 200: 113917.

[32] LEE T H, SIM M S, JOO S H, PARK K T, JEONG H G, LEE J H. Effect of intermetallic compound thickness on anisotropy of Al/Cu honeycomb rods fabricated by hydrostatic extrusion process [J]. Transactions of Nonferrous Metals Society of China, 2016, 26: 456−463.

[33] SHAYANPOOR A A, REZAEI-ASHTIANI H R. Constitutive model for hot deformation behaviors of Al/Cu bimetal composites based on their components [J]. Transactions of Nonferrous Metals Society of China, 2023, 33: 3641−3660.

[34] GUO Ya-jie, LIU Gui-wu, JIN Hai-yun, SHI Zhong-qi, QIAO Guan-jun. Intermetallic phase formation in diffusion-bonded Cu/Al laminates [J]. Journal of Materials Science, 2011, 46: 2467−2473.

[35] HAIDARA F, MANGELINCK D, DUPLOYER B, RECORD M C. Phase formation of $Al_{10}Cu_{10}Fe$ in thin films [J]. Materials Chemistry and Physics, 2012, 133: 977−980.

[36] HUA Fu-an, SONG Hong-wu, SUN Tao, LI Jian-ping. Inter-diffusion based analytical model for growth kinetics of IMC layers at roll bonded Cu/Al interface during annealing

process [J]. Metals and Materials International, 2020, 26: 333−345.
[37] LEE K E, LEE S E, KWON Y N. Interface characterization of Al/Cu 2-ply composites under various loading conditions [J]. Transactions of Nonferrous Metals Society of China, 2014, 24(Suppl.): 36−41.

热压烧结制备铝/铜多层复合材料的界面结构与力学性能

沈凯强[1,2]，陈 良[1,2]，钱丽华[1,2]，阚标华[1,2]，张存生[1,2]

1. 山东大学 材料液固结构演变与加工教育部重点实验室，济南 250061；
2. 山东大学 材料科学与工程学院，济南 250061

摘 要：以铜片和铝粉为原材料，基于热压烧结制备了铝/铜多层复合材料。研究了烧结参数对界面结构和力学性能的影响规律。结果表明，铝铜之间形成了结合质量良好的均匀界面。在 620 ℃下烧结 2 h，金属间化合物的厚度达到 33.88 μm；而当在 600 ℃烧结 1 h 时，其厚度仅为 14.88 μm。随烧结时间的延长，Al_4Cu_9 和 Al_2Cu 两相反应生成 AlCu 相，且 AlCu/Al_4Cu_9 界面处形成了一条非晶态氧化带。铝/铜多层材料的抗拉强度受晶粒形貌和界面结构的影响，而其拉伸断裂模式与界面结合强度密切相关。当在 600 ℃烧结 1 h 时，复合材料的抗拉强度和结合强度达到最高，其值分别为 151.1 和 93.7 MPa。

关键词：铝/铜多层复合材料；界面；金属间化合物；结合强度；力学性能

(Edited by Wei-ping CHEN)